Available online at www.sciencedirect.com
SCIENCE DIRECT®
International Journal of Heat and Mass Transfer 48 (2005) 4019–4027
International Journal of HEAT and MASS TRANSFER
www.elsevier.com/locate/ijhmt

Three-dimensional numerical simulation of an inclined jet with cross-flow

Yue-Tzu Yang *, Yong-Xun Wang

Department of Mechanical Engineering, National Cheng Kung University, Tainan 70101, Taiwan

Received 28 October 2004; received in revised form 1 April 2005
Available online 28 June 2005

Abstract

Three-dimensional numerical simulation of fluid flow and heat transfer characteristics for an inclined jet with cross-flow impinging on a heating plate is presented. The turbulent governing equations are solved by a control-volume-based finite-difference method with power-law scheme and the well-known k–ε turbulence model and its associate wall function to describe the turbulent structure. The velocity and pressure terms of momentum equations are solved by SIMPLE method. In addition, body fitted curvilinear coordinates system is employed. The parameters studied include the same inlet temperature of cross-flow and inclined jet (T_{in} = 30 and 40 °C), the inclined impinging jet to cross-flow velocity ratio (VR = 3–7), the heat flux (q''_w = 340–1000 W/m^2), the Reynolds number of the cross-flow and the angle between the inclined jet and the bottom surface are fixed at Re = 5000 and θ = 45°. The theoretical model developed is validated by comparing the predictions with available experimental data. The generation of a pair of counter-rotating longitudinal vortices is clearly observed from the computations. Heat transfer enhancement can be attained over wider span-wise region as the VR value is increased. The analysis provides a fundamental insight into the complex heat transfer characteristics for an inclined jet with cross-flow.

Keywords: Three-dimensional; Inclined jet; Cross-flow; Turbulence; Numerical simulation; Heat transfer

1. Introduction

Jet impingement can be found in many practical applications, e.g., cooling of turbine blades and electrical equipment, drying of paper, textiles, and annealing of metals. Several researches have studied the effect of cross-flow on the heat transfer characteristics of impinging turbulent jets [1–5]. Barata et al. [6] examined the characteristics of vortex and upwash flows generated by multiple jets in a cross-flow. Chuang et al. [7] used a two-dimensional numerical model to determine the flow characteristics associated with an unsteady, compressible impinging twin slot jets between two plates coupled with cross-flow. The numerical result of Al-Sanea [8] on single jet combined with cross-flow show that a cross-flow degrades the favorable characteristics of impinging jet. Kim and Benson [9] employed a turbulent model to simulate the three-dimensional impingement of multiple jets with cross-flow. Their results presented that the row of jets in the cross-flow is characterized by a highly complex flow field that includes a horseshoe vortex and two helical vortices whose secondary velocity components are

* Corresponding author. Tel.: +886 6 2757575x62172; fax: +886 6 2352973.
E-mail address: ytyang@mail.ncku.edu.tw (Y.-T. Yang).

0017-9310/$ - see front matter © 2005 Elsevier Ltd. All rights reserved.
doi:10.1016/j.ijheatmasstransfer.2005.04.018

Nomenclature

C_1, C_2, C_μ	turbulent constant
d	jet nozzle diameter
k	turbulent kinetic energy
Nu	Nusselt number
P	pressure
Pr	Prandtl number
q''_w	wall heat flux
Re	cross-flow Reynolds number
T	temperature
T_{in}	inlet temperature
U_{in}	inlet velocity
VR	velocity ratio of jet to cross-flow
u, v, w	velocity in the x-, y-, z-directions
x, y, z	streamwise, vertical and span-wise coordinate

Greek symbols

θ	angle between the inclined jet and the bottom surface
α	thermal diffusivity
ρ	density
μ_ℓ, μ_t	laminar and turbulent viscosity
ε	turbulent energy dissipation rate
σ_T	turbulent constant

co-rotating in space. The impingement of confined single and twin turbulent jets through a cross-flow has been studied experimentally and numerically by Barata et al. [10] to examine the characteristics of vortex and upwash flows generated by multiple jets in a cross-flow. Huang et al. [11] have studied various aspects of the jet impingement heat transfer under the influence of cross-flow. Nakabe et al. [12–14] investigated that Nusselt number distribution became a plateau-like pattern, which means that the enhanced region of heat transfer expanded more. The flow visualization demonstrated the generation of a pair of large-scale counter-rotating longitudinal vortices by an inclined impinging jet. In addition, gas turbine requires internal cooling of many components exposed to hot burnt gas flow, presented by Son et al. [15]. The most important requirement is to obtain uniform heat flux distributions which could be used multiple impinging jets. Fornalik et al. [16] investigated experimentally the flow patterns and heat transfer distributions of two kinds of geometrical arrangement of twin inclined jets. San and Lai [17] investigated experimentally of five confined circular air jets in staggered arrays vertically impinging on a flat plate. An optimum ratio of jet-to-jet spacing was obtained. Heat transfer from a discrete heat source to multiple, normally impinging, confined air jet was experimentally investigated by Garimella and Schroeder [18]. In this paper, the numerical simulations was employed to gain insight into the fluid flow and heat transfer characteristics of inclined jet with cross-flow impinging on a heated plate. The effect of jet to cross-flow velocity ratio on the flow and thermal fields is investigated.

2. Mathematical formulation

The schematic diagram of the geometry and the computational domain is shown in Fig. 1. It involves the three-dimensional heat transfer and fluid flow characteristics of turbulent flow in rectangular duct of an inclined jet with cross-flow. The turbulent three-dimensional Navier–Stokes and energy equations are solved numerically (using finite-difference scheme) combined with the continuity equation to simulate the thermal and turbulent flow fields. An eddy viscosity model is used to account for the effects of turbulence. The flow is assumed to be steady, incompressible, and three-dimensional. In addition, the thermophysical properties of the fluid are assumed to be constant.

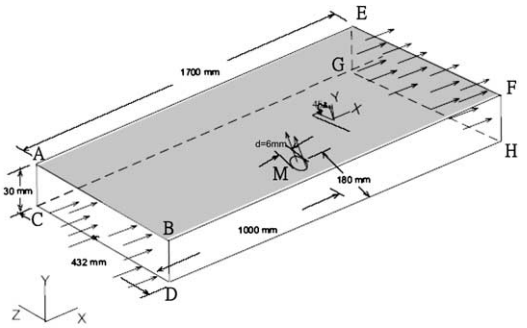

Fig. 1. Physical coordinate system and boundary conditions.

The three-dimensional governing equations of mass, momentum, turbulent kinetic energy, turbulent energy dissipation rate, and energy in the steady turbulent flow using the standard k–ε model are as follows:

Continuity equation

$$\frac{\partial \rho \overline{u_i}}{\partial x_i} = 0 \tag{1}$$

Momentum equation

$$\rho \overline{u_j} \frac{\partial \overline{u_i}}{\partial x_i} = -\frac{\partial \overline{p}}{\partial x_i} + \frac{\partial}{\partial x_j}\left[\mu_t\left(\frac{\partial \overline{u_i}}{\partial x_j} + \frac{\partial \overline{u_j}}{\partial x_i}\right)\right] \tag{2}$$

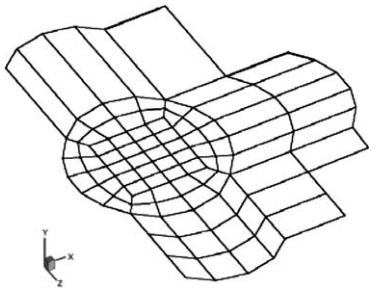

Fig. 2. The cross-sectional grid of the inclined jet.

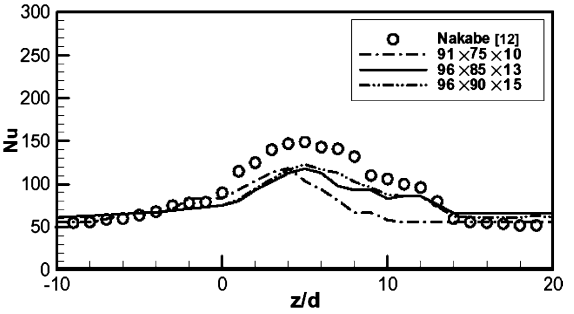

Fig. 3. Effect of grid refinement (VR = 5, $x/d = 20$).

Turbulent kinetic energy equation

$$\rho\overline{u_j}\frac{\partial k}{\partial x_j} = \frac{\partial}{\partial x_j}\left(\frac{\mu_t}{\sigma_k}\frac{\partial k}{\partial x_j}\right) + \mu_t\left(\frac{\partial \overline{u_i}}{\partial x_j} + \frac{\partial \overline{u_j}}{\partial x_i}\right)\frac{\partial \overline{u_i}}{\partial x_j} - \rho\varepsilon \tag{3}$$

Dissipation rate of turbulent kinetic energy

$$\rho\overline{u_j}\frac{\partial \varepsilon}{\partial x_j} = \frac{\partial}{\partial x_j}\left(\frac{\mu_t}{\sigma_\varepsilon}\frac{\partial \varepsilon}{\partial x_j}\right) + C_1\mu_t\frac{\varepsilon}{k}\left(\frac{\partial \overline{u_i}}{\partial x_j} + \frac{\partial \overline{u_j}}{\partial x_i}\right)\frac{\partial \overline{u_i}}{\partial x_j} - C_2\rho\frac{\varepsilon^2}{k} \tag{4}$$

Energy equation

$$\rho\overline{u_j}\frac{\partial \overline{T}}{\partial x_j} = \frac{\partial}{\partial x_j}\left[\left(\frac{\mu_\ell}{Pr} + \frac{\mu_t}{\sigma_T}\right)\frac{\partial \overline{T}}{\partial x_j}\right] \tag{5}$$

where $\mu_t = \rho C_\mu \frac{k^2}{\varepsilon}$.

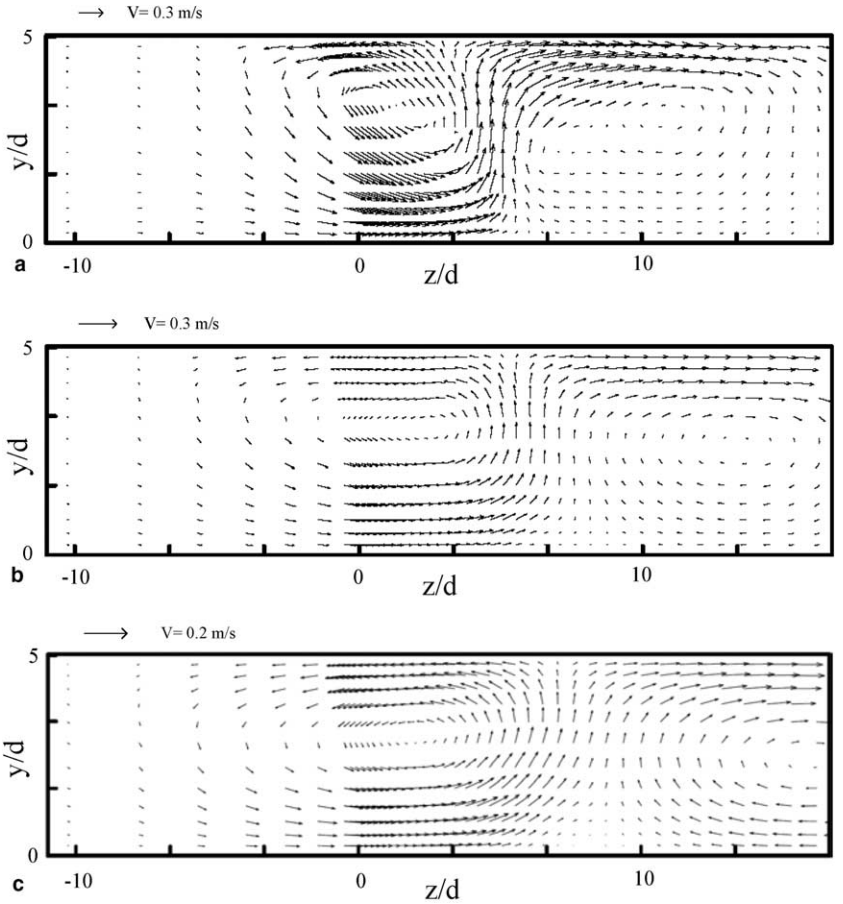

Fig. 4. (a) Velocity vector for $x/d = 10$, $Re = 5000$, VR = 7, $T_{in} = 30$ °C, $q''_w = 10^3$ W/m^2. (b) Velocity vector for $x/d = 20$, $Re = 5000$, VR = 7, $T_{in} = 30$ °C, $q''_w = 10^3$ W/m^2. (c) Velocity vector for $x/d = 40$, $Re = 5000$, VR = 7, $T_{in} = 30$ °C, $q''_w = 10^3$ W/m^2.

The empirical constants appear in the above equations are given by the following values: $C_\mu = 0.09$, $C_1 = 1.92$, $\sigma_k = 1.0$, $\sigma_\varepsilon = 1.3$ and $\sigma_T = 1.0$.

Boundary conditions for velocities: the cross-flow velocity is assumed to have an uniform profile at the inlet. The outlet boundary is located far enough downstream for conditions to be fully developed. For the near-wall region the law of the wall is assumed to be valid for both the flow and temperature fields. It is assumed that the region near the wall consists of only two layers. The point $y^+ = 11.63$ is usually defined to dispose the intersection between these two layers. Below this point the flow is assumed to be purely viscous, and above this point the flow is assumed to be purely turbulent. A no-slip boundary condition is imposed on the velocity components at the walls.

Boundary conditions for temperature: the inlet temperature of the cross-flow is assumed 30 and 40 °C. The adiabatic boundary condition is imposed on the bottom and side walls. The constant heat flux boundary condition is applied on the top wall.

3. Numerical computation

The numerical computation was carried out by solving the governing conservation equations with the boundary conditions. In this study, the computational domain was chosen to be larger than the physical domain to eliminate the entrance and exit effects and to satisfy continuity at the exit. A non-uniform grid system with a large concentration of nodes in regions of steep gradients, such as those close to the walls and inclined jet was employed. A structured computational mesh near the inclined jet was created as shown in Fig. 2. The mesh consisted of uniformly spaced grid divisions in a rectangular region around the center of the inclined jet. The numerical method used in the present study is based on the

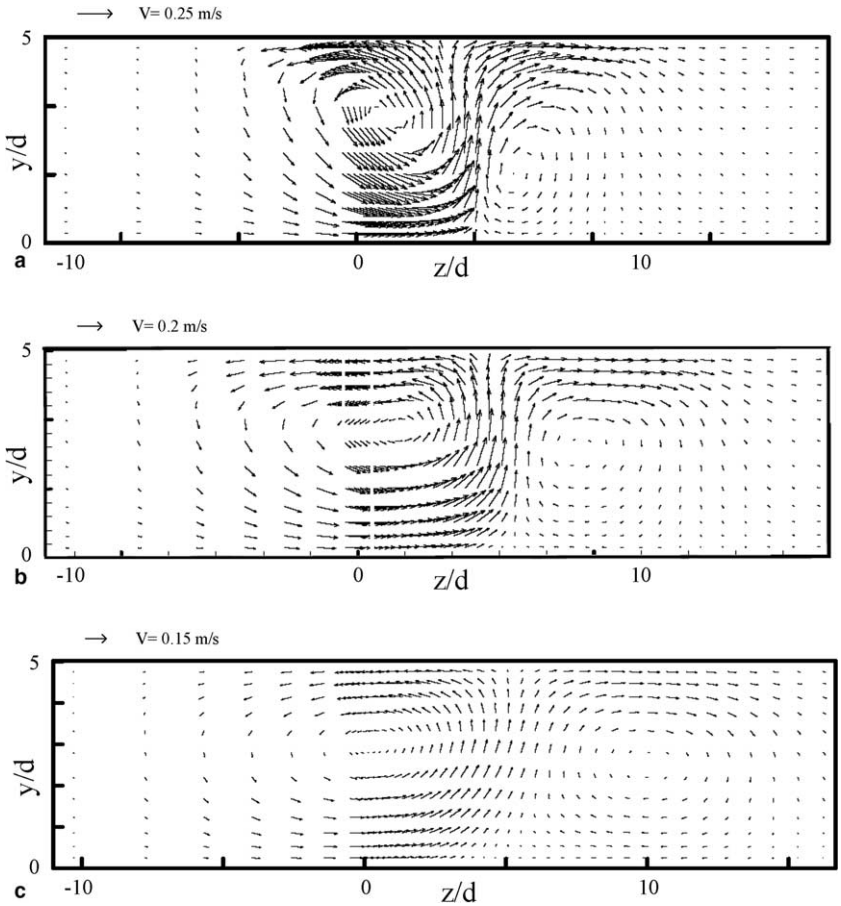

Fig. 5. (a) Velocity vector for $x/d = 10$, $Re = 5000$, VR = 5, $T_{in} = 30$ °C, $q''_w = 10^3$ W/m^2. (b) Velocity vector for $x/d = 20$, $Re = 5000$, VR = 5, $T_{in} = 30$ °C, $q''_w = 10^3$ W/m^2. (c) Velocity vector for $x/d = 40$, $Re = 5000$, VR = 5, $T_{in} = 30$ °C, $q''_w = 10^3$ W/m^2.

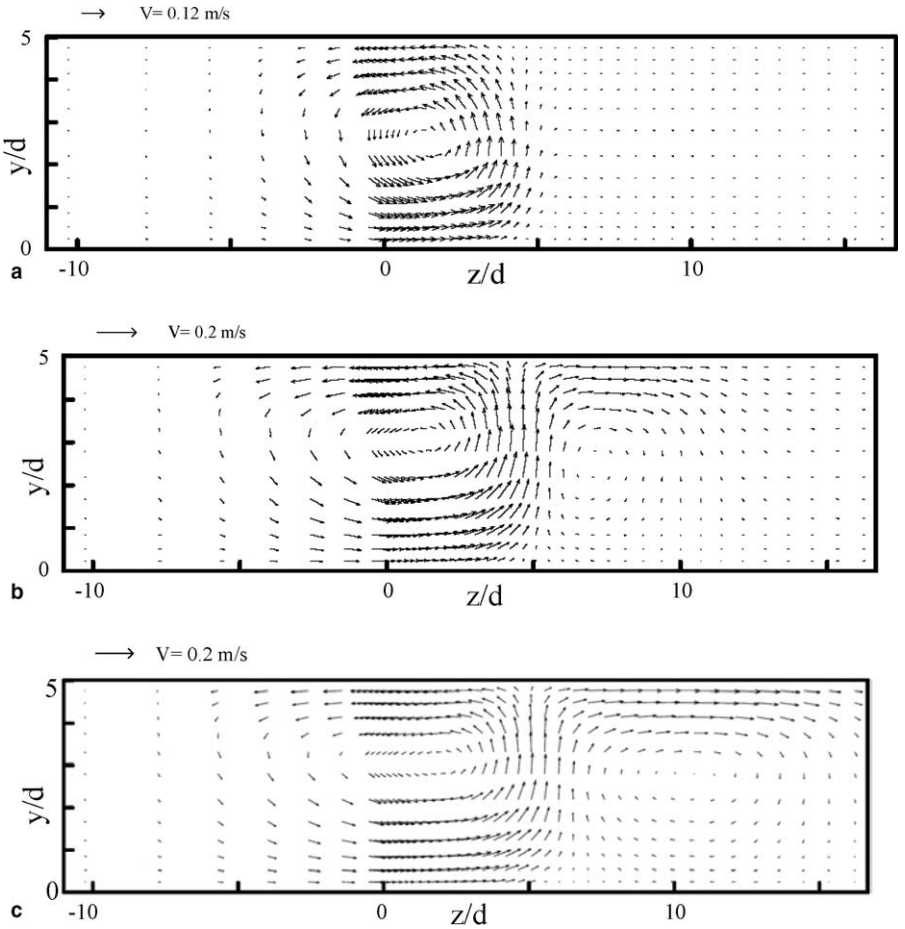

Fig. 6. (a) Velocity vector for VR = 3, $x/d = 20$, $Re = 5000$, $T_{in} = 40$ °C, $q''_w = 10^3$ W/m^2. (b) Velocity vector for VR = 5, $x/d = 20$, $Re = 5000$, $T_{in} = 40$ °C, $q''_w = 10^3$ W/m^2. (c) Velocity vector for VR = 7, $x/d = 20$, $Re = 5000$, $T_{in} = 40$ °C, $q''_w = 10^3$ W/m^2.

SIMPLE algorithm of Patankar [19]. This is an iterative solution procedure where the computation is begun by guessing the pressure field. The momentum equation is solved to determine the velocity components. Even though the continuity equation does not contain any pressure, it can be transformed easily into a pressure correction equation. The conservation equations are discretized by control-volume-based finite-difference method with power-law scheme. The set of difference equations are solved iteratively using a line by line solution method in conjunction with a tridiagonal matrix form. The solution is considered to be converged when the normalized residual of the algebraic equation is less than a prescribed value of 10^{-4}. The distribution of cells in the computational domain was determined from a series of tests with a different number of cells in the x-, y-, and z-directions. The results are shown in Fig. 3, which plots the Nu distribution along z/d for VR = 5, and $x/d = 20$. The grid structure with $91 \times 75 \times 10$ cells was not enough to capture all the changes, so finer grid structure was tested. The comparison of theoretical predictions with the experimental data was used to assess the grid independence of the results. The CPU time as well as memory storage required for performing three-dimensional calculations increase dramatically as the number of grid nodes increases even slightly. This needs to search for the number grid with the smallest possible number of nodes but still satisfying the acceptable accuracy requirements. Different size meshes, $91 \times 75 \times 10$, $96 \times 85 \times 13$ and $96 \times 90 \times 15$ in x-, y-, and z-directions, respectively, were employed in testing the numerical model. The results of the grid sensitivity study showed that the simulations based on the grid with 96 nodes in the x-direction, 85 nodes in the y-direction, and 13 nodes in the z-direction provide satisfactory numerical accuracy and are essentially grid independent. It has been validated using experimental data reported in the literature [12], and a good agreement has been found between the model predictions and measurements. These computations performed on IBM-RS6000, taken about 900–7200 s CPU time.

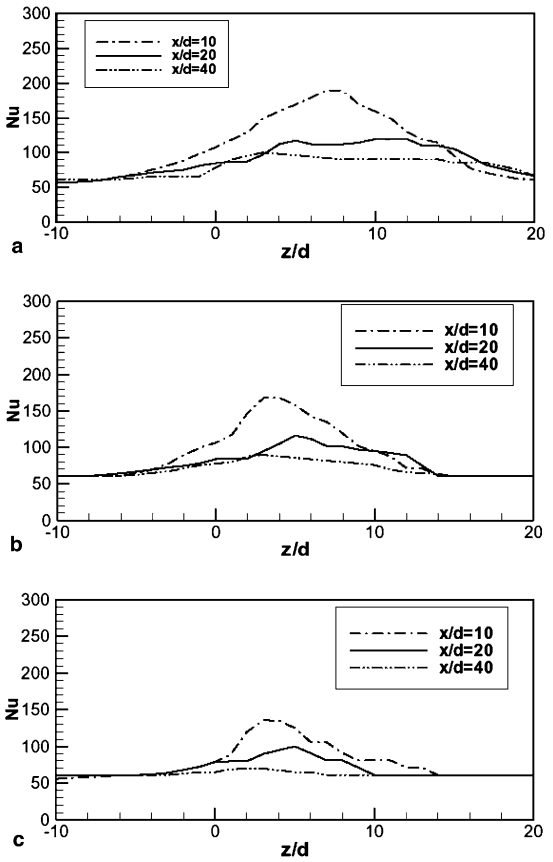

Fig. 7. *Nu* distribution: (a) VR = 7, Re = 5000, T_{in} = 30 °C, q''_w = 10^3 W/m^2; (b) VR = 5, Re = 5000, T_{in} = 30 °C, $q''_w = 10^3$ W/m^2 and (c) VR = 3, Re = 5000, T_{in} = 30 °C, $q''_w = 10^3$ W/m^2.

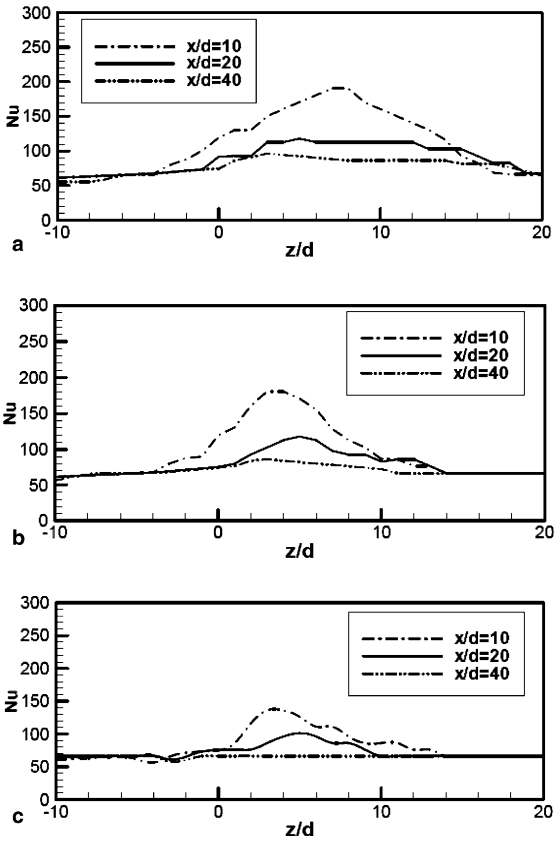

Fig. 8. *Nu* distribution: (a) VR = 7, Re = 5000, T_{in} = 30 °C, q''_w = 340 W/m^2; (b) VR = 5, Re = 5000, T_{in} = 30 °C, q''_w = 340 W/m^2 and (c) VR = 3, Re = 5000, T_{in} = 30 °C, q''_w = 340 W/m^2.

4. Results and discussion

The numerical algorithm and computer program were carefully evaluated by comparing model prediction with available experimental data for inclined jet with cross-flow [12]. Reference to Nakabe et al. [12], the test section was 432 mm wide and 30 mm high. The jet diameter was 6 mm. The height of the test section is five times the nozzle diameter. The cross-flow Reynolds number based on the time-averaged cross-flow velocity at the inlet, and the hydraulic diameter of the channel were kept constantly equal to 5000. The jet to cross-flow velocity ratio VR = 3, 5 and 7. In the computations and experiments of Nakabe et al. [12], water was used as a working fluid with the inlet temperature T_{in} = 30 and 40 °C. An uniform heat flux of q''_w = 340–1000 W/m^2 was imposed at the top wall.

Fig. 4a–c shows the velocity vector for the case of VR = 7 at three different streamwise locations. The secondary flow velocity vector for the corresponding cases are shown for comparison. A pair of counter-rotating vortices are clearly seen in the figure; one with anti-clockwise rotation is found at an almost constant span-wise location around z/d = 0, and the other with clockwise rotation is shift a little in the span-wise direction toward a position, z/d = 10 for the case of x/d = 10, z/d = 13, for the case of x/d = 20, and also around z/d = 15 for the case of x/d = 40. The velocity vectors for the case of VR = 5 at three different streamwise locations are shown in Fig. 5a–c. The anti-clockwise-rotating longitudinal vortex of positive streamwise vorticity is situated at almost the same position around z/d = 1–2 in all cases. The other vortex in the clockwise rotation is clearly observed around z/d = 6–10 for the case of VR = 5. This vortex induces strong span-wise flow sweeping the top wall surface. The velocity vector for three different values of the velocity ratio, VR = 3, 5 and 7 at x/d = 20 are shown in Fig. 6a–c. The anti-clockwise-rotating longitudinal vortex of positive streamwise vorticity is situated at almost the same position around z/d = 1–2 in all the cases. The other vortex having the

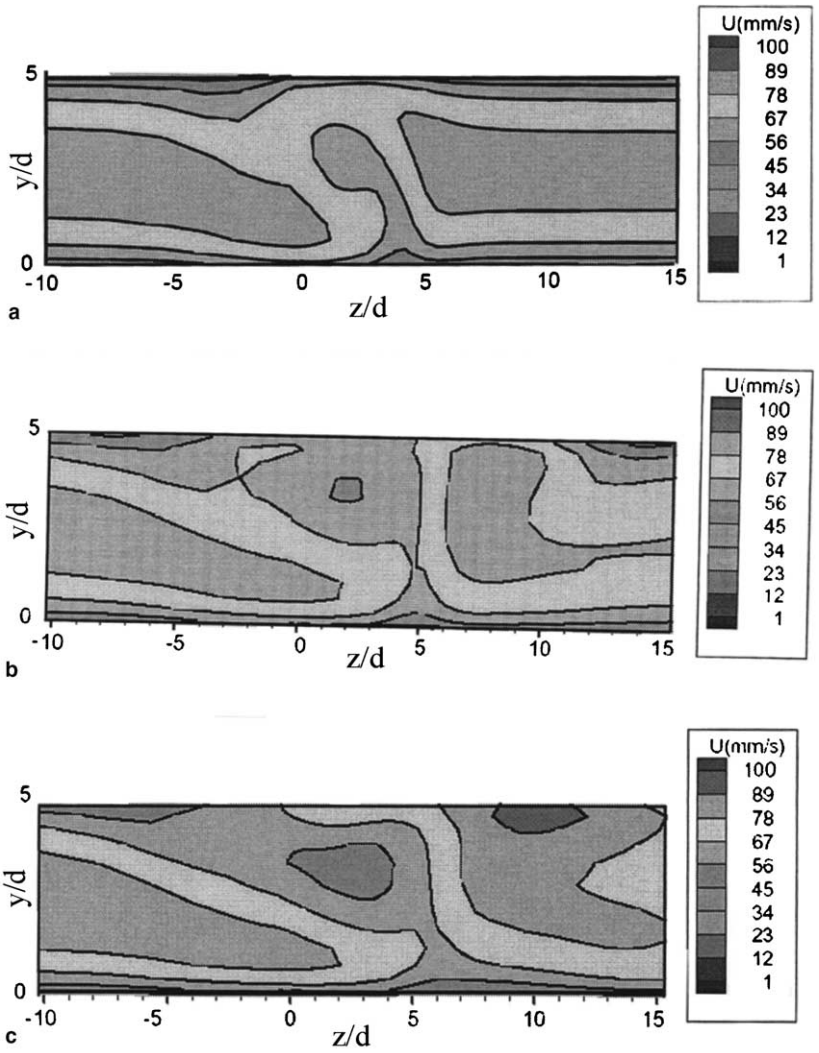

Fig. 9. U contours: (a) $x/d = 20$, VR = 3, $Re = 5000$, $T_{in} = 30\ ^{\circ}C$, $q''_w = 10^3\ W/m^2$; (b) $x/d = 20$, VR = 5, $Re = 5000$, $T_{in} = 30\ ^{\circ}C$, $q''_w = 10^3\ W/m^2$ and (c) $x/d = 20$, VR = 7, $Re = 5000$, $T_{in} = 30\ ^{\circ}C$, $q''_w = 10^3\ W/m^2$.

clockwise rotation is clearly observed around $z/d = 6$ for the case of VR = 5 and also around $z/d = 10$ for the case of VR = 7, but is weakened in the case of VR = 3. The position of the rotating vortex moves away from the nozzle position in z-direction as the VR is increased.

Fig. 7a–c shows the Nusselt number distributions for three different values of the velocity ratio, VR = 3, 5 and 7, but at the same streamwise location, $x/d = 20$. In the case of VR = 3, the span-wise position of the peak Nusselt number is located around $z/d = 4$, which corresponds to the region of the upwash flow mainly induced by the anti-clockwise vortex. It is found that the peak position of Nusselt number moves a little toward the right side wall of the duct with an increase in the VR value. The Nusselt number distribution exhibits a shape almost like a plateau in the wide range of the span-wise position from $z/d = 5$ to 18. Fig. 8a–c shows the span-wise distributions of Nusselt number at $q''_w = 340\ W/m^2$ for the case of VR = 7, 5 and 3 at three different streamwise locations. It can be noticed that the Nusselt number decreases about 5–10% at low heat flux $q''_w = 340\ W/m^2$. Comparison between the Nusselt number distributions and the velocity vector shows that the enhanced region of heat transfer corresponds very well to the locations of the counter-rotating longitudinal vortices. The secondary flow velocity in the cross-section becomes smaller downstream. Following this decrease of the velocity, Nusselt number in the whole enhanced region also decreases along the streamwise direction.

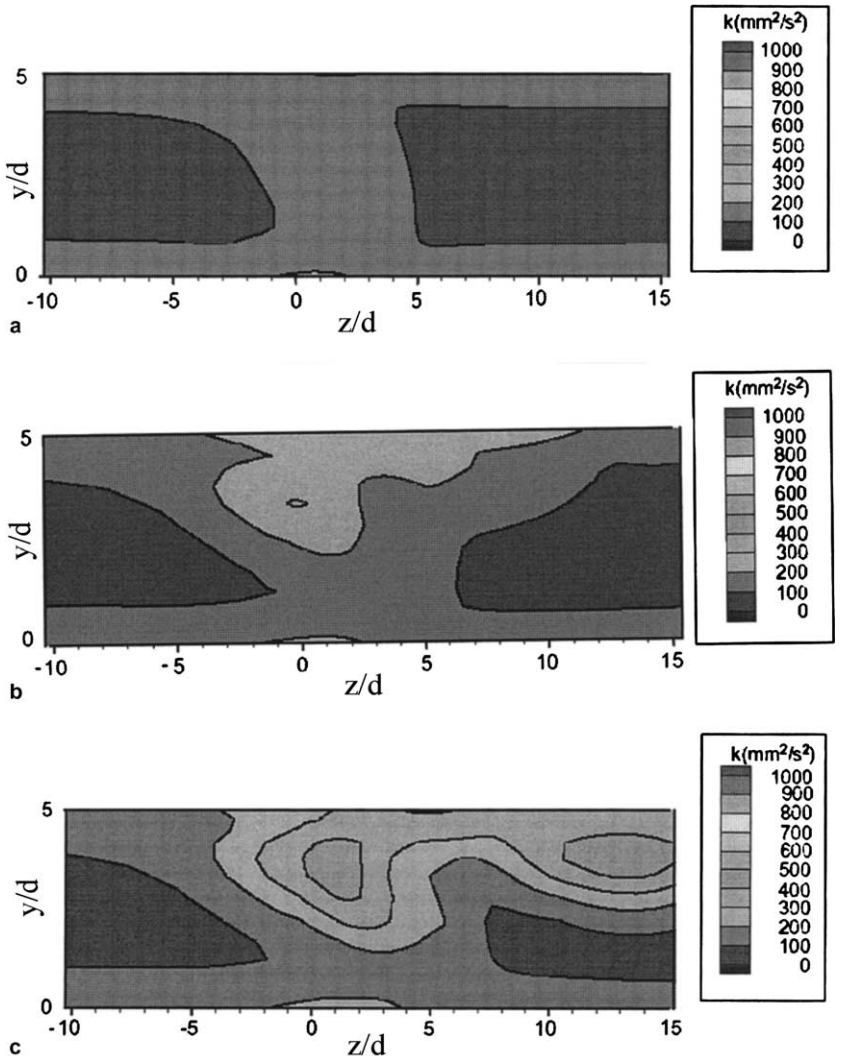

Fig. 10. Contours of turbulent kinetic energy: (a) $x/d = 20$, VR = 3, $T_{in} = 30$ °C, $Re = 5000$; (b) $x/d = 20$, VR = 5, $T_{in} = 30$ °C, $Re = 5000$ and (c) $x/d = 20$, VR = 7, $T_{in} = 30$ °C, $Re = 5000$.

Heat transfer enhancement can be attained over wider span-wise region as the VR value is increased. This expansion of the high Nusselt number region is caused by the high streamwise velocity flow combined with span-wise flows sweeping the surface of the target plate, which are produced by the clockwisely rotating longitudinal vortex. Fig. 9a–c shows the contours of the time-averaged streamwise velocity U for three different cases of VR = 3, 5 and 7. In the case of VR = 3, a small velocity region appears near the top wall surface just on the left side of $x/d = 0$. The low velocity region expands wider as the VR value is increased. A more important phenomena observed in this figure is that a higher streamwise velocity region exists just on the left side of the clockwise-rotating longitudinal vortex. The high velocity region is present very near the surface of the top wall so that this should be related to the increase of the Nusselt number on the right side of its peak. Turbulent kinetic energy has large values in two regions corresponding very well to the positions of a pair of centers of the counter-rotating longitudinal vortices as clearly seen in Fig. 10a–c.

5. Conclusions

The theoretical analysis performed, provides a fundamental understanding of the fluid flow and heat transfer characteristics for an inclined jet with cross-flow impinging on a heated plate. A three-dimensional mathematical

model, developed using incompressible turbulent Navier–Stokes equations of motion and energy equation, is capable of predicting correctly the flow and heat transfer characteristics for an inclined jet with cross-flow impinging on a heated plate. In the flow structure, a pair of counter-rotating longitudinal vortices was clearly observed; one having anti-clockwise rotation is situated around $z/d = 0$ regardless of the VR value, and the other having clockwise rotation moves away from the nozzle position in the z-direction with an increase in the VR value. Heat transfer enhancement can be found over wider span-wise region as the VR value is increased. The peak Nusselt number located around $z/d = 4$, which is caused by the upwash region supplying fresh fluid to the near region of the target plate surface. It has been validated using experimental data reported in the literature, and a good agreement has been found.

References

[1] D.E. Metzger, R.J. Korstad, Effects of crossflow on impingement heat transfer, ASME J. Eng. Power 94 (1972) 35–42.

[2] J.P. Bouchez, R.J. Goldstein, Impingement cooling from a circular jet in a cross flow, Int. J. Heat Mass Transfer 18 (1975) 719–730.

[3] E.M. Sparrow, R.J. Goldstein, M.A. Rouf, Effect of nozzle-surface separation distance on impingement heat transfer for a jet in a crossflow, ASME J. Heat Transfer 97 (1975) 528–533.

[4] N.R. Saad, A.S. Mujumdar, W.A. Messeh, W.J.M. Douglas, Local heat transfer characteristics for staggered arrays of circular impinging jets with cross-flow of spent air, ASME paper 80-TH-23, 1980, pp. 105–112.

[5] R.J. Goldstein, A.I. Behbahani, Impingement of a circular jet with and without crossflow, Int. J. Heat Mass Transfer 25 (1982) 1377–1382.

[6] J.M.M. Barata, D.F.G. Durao, M.V. Heitor, Impingement of single and twin turbulent jets, AIAA J. 29 (1991) 595–602.

[7] S.H. Chuang, M.H. Chen, S.W. Lii, F.M. Tai, Numerical simulation of twin-jet impingement on a flat plate coupled with cross-flow, Int. J. Numer. Methods Fluids 14 (1992) 459–475.

[8] S. Al-Sanea, A numerical study of the flow and heat transfer characteristics of an impinging laminar slot jet including crossflow effects, Int. J. Heat Mass Transfer 35 (1992) 2501–2513.

[9] S.W. Kim, T.J. Benson, Fluid flow of a row of jets in crossflow—a numerical study, AIAA J. 31 (1993) 806–811.

[10] J.M.M. Barata, Fountain flows produced by multiple impinging jets in a crossflow, AIAA J. 34 (1996) 2523–2530.

[11] Y. Huang, S.V. Ekkad, J.C. Han, Detailed heat transfer coefficient distributions under an array of inclined impinging jets using a transient liquid crystal technique, in: Ninth International Symposium on Transport Phenomena II, 1996, pp. 807–812.

[12] K. Nakabe, K. Suzuki, K. Inaoka, A. Higashio, J.S. Acton, W. Chen, Generation of longitudinal vortices in internal flows with an inclined impinging jet and enhancement of target plate heat transfer, Int. J. Heat Fluid Flow 19 (1998) 573–581.

[13] K. Nakabe, A. Higashio, W. Chen, K. Suzuki, J.H. Kim, An experimental study on the flow and heat transfer characteristics of longitudinal vortices induced by an inclined impinging jet into a crossflow, in: 11th International Heat Transfer Conference, vol. 5, 1998, pp. 439–444.

[14] K. Nakabe, Y. Yamamoto, E. Fornalik, W. Chen, K. Suzuki, Visualizations of obliquely discharged jet flows and their heat transfer enhancement regions, in: CD-rom of Eighth International Symposium on Flow Visualization, Italy, 1998 (ISBN 0953399109).

[15] J.W. Son, G.H. Kwan, J.L. Sohn, Measurement of heat transfer coefficients inside turbine cooling blades in gas turbine engine using thermal imagine technique, in: Third KSME/JSME Thermal Engineering Conference, Kyongju, Korea III-89-III-92, 1996.

[16] E. Fornalik, K. Nakabe, Y. Yamamoto, W. Chen, K. Suzuki, Visualizations of heat transfer enhancement regions modified by the interaction of inclined impinging jets into crossflow, Machine Graphics Vis. 8 (1999) 597–610.

[17] J.Y. San, M.D. Lai, Optimum jet-to-jet spacing of heat transfer for staggered arrays of impinging air jets, Int. J. Heat Mass Transfer 44 (2001) 3997–4007.

[18] S.V. Garimella, V.P. Schroeder, Local heat transfer distributions in confined multiple air jet impingement, ASME J. Electron. Packag. 123 (2001) 165–172.

[19] S.V. Patankar, Numerical Heat Transfer and Fluid Flow, McGraw-Hill, New York, 1980.